Dynamical properties of lasers coupled face to face

J. Javaloyes
Institut Non Linéaire de Nice, UMR 6618 CNRS-UNSA, 1361 Route des Lucioles, F-06560 Valbonne, France

Paul Mandel and D. Pieroux
Optique Nonlinéaire Théorique, Université Libre de Bruxelles, Campus Plaine CP 231, B-1050 Bruxelles, Belgium

(Received 14 June 2002; revised manuscript received 19 November 2002; published 10 March 2003)

We derive a reduced model to describe two identical lasers coupled face to face. Two limits are introduced in the Maxwell-Bloch equations: adiabatic elimination of the material polarization and large distance between the two lasers. The resulting model describes coupled homogeneously broadened lasers, including semiconductor lasers. It consists of two coupled delay differential equations with delayed linear cross-coupling and an instantaneous self-coupling nonlinearity. The study is analytical and numerical. We focus on the properties of steady and periodic amplitudes of the electric fields. In steady state, there are symmetric, antisymmetric, and asymmetric solutions with respect to a permutation of the two fields. A similar classification holds for the periodic states. The stability of these solutions is determined partly analytically and partly numerically. A homoclinic point is associated with the asymmetric periodic solutions.

DOI: 10.1103/PhysRevE.67.036201 PACS number(s): 05.45.−a, 42.65.Sf, 42.60.Mi, 42.55.Px

I. INTRODUCTION

This paper deals with the nonlinear dynamics of two semiconductor lasers coupled face to face (F2F): the output of each laser is injected, after a suitable attenuation, in the other laser. The emphasis will be on the influence of the unavoidable delay due to the transit time between the two lasers. The subject of F2F coupling is not popular in experimental laser physics because the injection of a signal in an amplifier is a fine source of instabilities which are difficult to control. Few studies have been made for gas or solid-state lasers in that configuration. However, with the emergence of chaos synchronization studies in semiconductor lasers motivated by the prospect of transmitting coded information [1], two important factors that hampered the study of the F2F configuration have turned out to be useful sources of new physics: (i) the injected field induces chaos since the isolated lasers are operating in a stable regime; (ii) the delay which is the propagation time between the two lasers has considerable influence on the nonlinear dynamics by introducing a new and easily controllable time scale in the system. Its relevance is also related to the fact that, for semiconductor lasers, the distance between the two lasers is usually much larger than the laser dimensions. Although the derivation of the model equations will be quite general and not tied to a particular type of laser, the choice of values for the parameters in the figures will be for semiconductor lasers.

Stable localized synchronization of two different semiconductor lasers coupled F2F was demonstrated in the periodic and quasiperiodic regimes [2]. More recently, synchronization of two identical semiconductor lasers coupled F2F and operating in a chaotic regime was reported [3]. Some formal aspects of synchronization in the F2F configuration have been considered [4].

Independently of these studies, which specifically focus on semiconductor lasers, there has been a large amount of research on the influence of the delay in the theory of coupled nonlinear oscillators with an emphasis on the Kuramoto model [5,6]. Coupled nonlinear oscillators with a time delay may display multistability [7], delay-induced ''death'' in which one oscillator prevents the periodic regime in the other oscillator [8], and stochastic resonance [9]. Analytical expressions for the boundaries of synchronized regimes were obtained in Ref. [10]. The relevance of these studies to the physics of semiconductor lasers follows from the proof that the Lang-Kobayashi model for a single mode semiconductor laser with external feedback [11] can asymptotically be reduced to a phase equation of which the Kuramoto equation is a particular limit [12]. This result was extended to an array of semiconductor lasers, with a systematic study of their synchronization properties [13,14].

In comparison with what is known in the theory of ordinary and partial differential equations, the mathematics of delay differential equations are underdeveloped due to the inherent difficulty associated with their structure. Few results are simple and little is known about generic properties of this class of equations. In a recent paper [15], it has been shown that in the long delay time limit, the two Lang-Kobayashi rate equations, which are the canonical description of a semiconductor laser with external feedback, may be reduced to a simpler problem which retains the essential features of the full model. That reduced model consists of a single delay differential equation with delayed linearity and instantaneous nonlinearity. The purpose of this paper is to extend that approach to the case of two coupled lasers in a F2F configuration.

This paper is organized as follows. In Sec. II, we show that, starting with the Maxwell-Bloch equations for two F2F coupled homogeneously broadened lasers, the reference model is asymptotically obtained by (i) adiabatically eliminating the material polarization, (ii) by introducing the long delay time limit. The inherent symmetry of the problem suggests several combinations of the electric fields. They are reviewed in Sec. IV. The steady state solutions, which are the equivalent of the external cavity modes of the Lang-

 ©2003 The American Physical Society

Kobayashi equations, are analyzed in Sec. V. Hopf bifurcations arise on these steady solutions and lead to periodic regimes which are analyzed in Sec. VI. These analytic results are complemented by a numerical study presented in Sec. VII and conclusions are drawn in Sec. VIII.

II. DERIVATION OF THE REFERENCE MODEL

We consider two single mode lasers, each of which is described by the usual Maxwell-Bloch equations for a homogeneously broadened laser. The output of each laser is injected in the other laser after a suitable attenuation. The Maxwell-Bloch equations couple the intracavity field $\tilde{\mathcal{E}}_j$ with the space average of the material polarization $\tilde{\mathcal{S}}_j$ and inversion $\tilde{\mathcal{N}}_j$ of the active medium

$$\frac{d\tilde{\mathcal{E}}_j}{dt'} = -\kappa_j(1-i\Delta_j)\tilde{\mathcal{E}}_j - ig\tilde{\mathcal{S}}_j + \kappa_j\tilde{\epsilon}_j\tilde{\mathcal{E}}_{3-j}(t'-\tau'_{3-j}), \quad (1)$$

$$\frac{d\tilde{\mathcal{S}}_j}{dt'} = -\gamma_\perp(1-i\alpha_j)\tilde{\mathcal{S}}_j + ig\tilde{\mathcal{E}}_j\tilde{\mathcal{N}}_j, \quad (2)$$

$$\frac{d\tilde{\mathcal{N}}_j}{dt'} = -\gamma_\parallel(\tilde{\mathcal{N}}_j - \tilde{\mathcal{N}}_{eq}) + 2ig(\tilde{\mathcal{E}}_j^*\tilde{\mathcal{S}}_j - \tilde{\mathcal{S}}_j^*\tilde{\mathcal{E}}_j), \quad (3)$$

with $j=1$ or 2. The κ_j are the damping rates of the two lasing cavities and the Δ_j are their normalized frequency detuning. The parameters $\tilde{\epsilon}_j$ account for the attenuation of each field before being injected in the other laser. The finite distance between the two lasers and the finite velocity of light imply that the injected fields are delayed with respect to the emitted fields by $\tau_j = L_j/v$, where L_j is the optical length between laser j and laser $3-j$, and v is the light velocity between the two lasers. The active medium is characterized by the damping rates $\gamma_\perp$ and $\gamma_\parallel$, the atom-field interaction strength g which is chosen to be real and α_j is the field-matter frequency mismatch for a solid-state laser or the line enhancement factor for a semiconductor laser. Note that there is no generally accepted convention for the sign of α. This leads sometimes to apparent contradictions. It would be easy to generalize these equations to include different light velocities in each directions, different light-matter coupling parameters, and different material damping rates. Given the two asymptotic limits we shall introduce, this would not change the structure of the resulting reduced equations.

A first asymptotic limit introduced in this problem is based on the assumption that the polarization is a variable that relaxes much faster than the inversion or the field in any of the two lasers: $\gamma_\perp \gg \gamma_\parallel, \kappa_j$. We also assume that the difference between the two laser frequencies is much smaller than $\gamma_\perp$ so that the beat frequency is a slow variable. As a result, the material polarization can be adiabatically eliminated,

$$\tilde{\mathcal{S}}_j = \frac{ig(1+i\alpha_j)}{\gamma_\perp(1+\alpha_j^2)}\tilde{\mathcal{E}}_j\tilde{\mathcal{N}}_j.$$

The remaining dynamical equations (1)–(3) become

$$\frac{d\tilde{\mathcal{E}}_j}{dt'} = \kappa_j\left[\tilde{\mathcal{E}}_j\left(-1+i\Delta_j + \frac{g^2(1+i\alpha_j)}{\kappa_j\gamma_\perp(1+\alpha_j^2)}\tilde{\mathcal{N}}_j\right) + \tilde{\epsilon}_j\tilde{\mathcal{E}}_{3-j}(t'-\tau'_{3-j})\right], \quad (4)$$

$$\frac{d\tilde{\mathcal{N}}_j}{dt'} = \gamma_\parallel\left(\tilde{\mathcal{N}}_{eq} - \tilde{\mathcal{N}}_j - \frac{4g^2}{\gamma_\parallel\gamma_\perp(1+\alpha_j^2)}|\tilde{\mathcal{E}}_j|^2\tilde{\mathcal{N}}_j\right). \quad (5)$$

We assume that the photon lifetimes inside the cavities, $1/\kappa_j$, are identical. Therefore time can be usefully rescaled as $t=\kappa t'$ and $T=\kappa/\gamma_\parallel$ is the dimensionless lifetime of the carrier within the lasers. Consequently Eqs. (4) and (5) become

$$\frac{d\tilde{\mathcal{E}}_j}{dt} = \tilde{\mathcal{E}}_j\left(-(1-i\Delta_j) + \frac{g^2(1+i\alpha_j)}{\kappa_j\gamma_\perp(1+\alpha_j^2)}\tilde{\mathcal{N}}_j\right) + \tilde{\epsilon}_j\tilde{\mathcal{E}}_{3-j}(t-\tau_{3-j}),$$

$$\frac{d\tilde{\mathcal{N}}_j}{dt} = \frac{1}{T}\left(\tilde{\mathcal{N}}_{eq} - \tilde{\mathcal{N}}_j - \frac{4g^2}{\gamma_\parallel\gamma_\perp(1+\alpha_j^2)}|\tilde{\mathcal{E}}_j|^2\tilde{\mathcal{N}}_j\right).$$

As a last step, we rescale the dynamical variables and the feedback rates,

$$\tilde{\mathcal{N}}_j = \tilde{\mathcal{N}}_j^{(s)}(1+2\mathcal{N}_j) = (1+2\mathcal{N}_j)\gamma_\perp\kappa_j(1+\alpha_j^2)/g^2,$$

$$\tilde{\mathcal{E}}_j = \frac{1}{2g}\sqrt{2\gamma_\perp\gamma_\parallel(1+\alpha_j^2)}\mathcal{E}_j,$$

$$\tilde{\epsilon}_j = \epsilon_j\sqrt{(1+\alpha_j^2)/(1+\alpha_{3-j}^2)}.$$

We also define the new parameters

$$\tilde{\mathcal{N}}_{eq} = \tilde{\mathcal{N}}_j^{(s)}(1+2P_j), \nu_j = \Delta_j + \alpha_j,$$

where P_j is the excess pumping rate above threshold and ν_j the free running frequency of the laser j. All this leads to the set of equations

$$\frac{d\mathcal{E}_j}{dt} = (1+i\alpha_j)\mathcal{N}_j\mathcal{E}_j + i\nu_j\mathcal{E}_j + \epsilon_j\mathcal{E}_{3-j}(t-\tau_{3-j}),$$

$$\frac{d\mathcal{N}_j}{dt} = \frac{1}{T}[P_j - \mathcal{N}_j - (1+2\mathcal{N}_j)|\mathcal{E}_j|^2].$$

These equations have the form of two coupled Lang-Kobayashi equations if the α_j can be interpreted as fixed constants. Nevertheless, for a pair of solid-state lasers, the α_j are still functions of the unknown lasing frequency.

A further simplification is to assume that the two delays are identical, i.e., $\tau_j = \tau_{3-j} = \tau$. Following the analysis in Ref. [15], we introduce a scaling which is useful in the large delay limit,

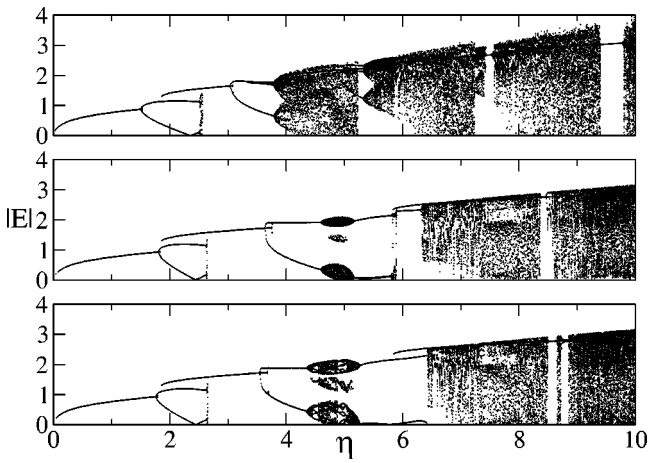

FIG. 1. Comparing the bifurcation diagrams obtained for T/τ small but finite and $T/\tau=0$. From top to bottom: $T/\tau=0.1,0.01$, and 0. In each diagram, the exterma of the solutions are plotted. For T/τ finite, Eqs. (7) and (8) are integrated. For $T/\tau=0$, Eqs. (9) and (10) are integrated.

$$E_j=\sqrt{\tau}\mathcal{E}_j,\ N_j=\tau\mathcal{N}_j,\ p_j=P_j/\tau,\ \eta_j=\tau\epsilon_j,$$
$$s=t/\tau,\ \Omega_j=\tau\nu_j. \tag{6}$$

It yields

$$\dot{E}_j=(1+i\alpha_j)N_jE_j+i\Omega_jE_j+\eta_jE_{3-j}(s-1), \tag{7}$$

$$\frac{T}{\tau}\dot{N}_j=p_j-N_j-\left(1+\frac{2}{\tau}N_j\right)|E_j|^2, \tag{8}$$

where the dot denotes the derivative with respect to the dimensionless time s.

A second asymptotic limit is the long delay time limit $1/\tau\to 0$, which leads to a substantial simplification of Eq. (8) since it reduces to $N_j=|E_j|^2-p_j$. Inserting this relation into the field equations (7) leads to

$$\dot{E}_1=(1+i\alpha_1)(p_1-|E_1|^2)E_1+i\Omega_1E_1+\eta_1\overline{E}_2, \tag{9}$$

$$\dot{E}_2=(1+i\alpha_2)(p_2-|E_2|^2)E_2+i\Omega_2E_2+\eta_2\overline{E}_1, \tag{10}$$

with the notation $\overline{E}_j(s)\equiv E_j(s-1)$.

To estimate the validity of the above asymptotic limit, we constructed numerically the bifurcation diagram of Eqs. (7) and (8) for two values of the ratio T/τ and the bifucration diagram of Eqs. (9) and (10). The result is shown in Fig. 1. Starting with $\eta=10^{-3}$ and a random initial condition, we integrate over 500 delay times to let the system reach its final state. We then record the extrema, that is, the intensities at which their time derivative cross the zero value. Then, η is slightly increased and the procedure is repeated until $\eta=10$. Then, we repeat the procedure beginning with $\eta=10$ and decreasing η. The numerical time integration used a modified fourth order Runge-Kutta method with linear interpolation of the delayed term, which gives a second order overall accuracy.

With $\kappa=10^{12}$ and $\gamma_\parallel=10^9$, the parameter T is equal to 10^3. Accordingly, we chose $\tau=\kappa\tau'$ equal to 10^4 and 10^5, corresponding to a propagation length (in vacuum) of 3 and 30 meters, respectively. The agreement between the bifurcation diagrams obtained with $T/\tau=10^{-2}$ and $T/\tau=0$ is very good.

To make contact with a more standard form of the model equations, the fields will be described in a reference frame rotating at the mean velocity $\Omega=(\Omega_1+\Omega_2)/2$. It is useful to introduce the mean and the mismatch functions

$$x\equiv\frac{1}{2}(x_1+x_2),$$

$$\delta x\equiv\frac{1}{2}(x_1-x_2),$$

where x is any of the parameters η_j,α_j,p_j, or Ω_j. This leads from Eqs. (9) and (10) to the equations

$$\dot{E}_1=(1+i\alpha)(p-|E_1|^2)E_1+\eta e^{-i\Omega}\overline{E}_2+\delta F_1(E_1,\overline{E}_2), \tag{11}$$

$$\dot{E}_2=(1+i\alpha)(p-|E_2|^2)E_2+\eta e^{-i\Omega}\overline{E}_1+\delta F_2(E_2,\overline{E}_1), \tag{12}$$

where the functions δF_1 and δF_2 have been defined as

$$\delta F_1(E_1,\overline{E}_2)\equiv i\delta\alpha\delta pE_1+[\delta\eta e^{-i\Omega}\overline{E}_2+i\delta\Omega E_1+\delta p(1+i\alpha)E_1+i\delta\alpha(p-|E_1|^2)E_1], \tag{13}$$

$$\delta F_2(E_2,\overline{E}_1)\equiv i\delta\alpha\delta pE_2-[\delta\eta e^{-i\Omega}\overline{E}_1+i\delta\Omega E_2+\delta p(1+i\alpha)E_2+i\delta\alpha(p-|E_2|^2)E_2]. \tag{14}$$

Equations (11) and (12) are two cross-coupled delay differential equations plus a perturbation δF_j which vanishes if the two lasers are identical. In that case, there is an obvious analogy with the reduced equation

$$\dot{E}=(1+i\alpha)(p-|E|^2)E+\eta e^{-i\Omega}\overline{E} \tag{15}$$

derived in the same long delay time limit from the Lang-Kobayashi equations [15].

III. PHYSICAL DISCUSSION

An experimental setup has to match the two main hypotheses of the present study, as detailed in Sec. II: the long delay limit with respect to the characteristic times constants of the lasers, and negligible retroreflection at the laser mirrors, since we are interested here only in mutual injection and not in feedback effects.

The former can be achieved by coupling the two lasers via a long single mode telecom fiber whose length should be of the order of 10 m if semiconductor lasers are used. Moreover, unavoidable losses due to propagation effects are not a

problem here, since we only need an injection ratio of the order of a few percent. As a consequence, the use of a neutral density filter (NDF) is also needed in order to control the coupling strength between the two lasers.

The latter hypothesis can be fulfilled by placing a antifeedback (AF) device between each laser and the fiber. An AF system will be composed, starting from the emitting face of each laser, of a quarter wave plate with its axis oriented at 45° with respect to a polarizer following it. Doing this, light entering parallel to the polarizer will end up perpendicular to it after a first passage through the quarter wave plate, a reflection, and a second passage through the quarter wave plate. Doing this, feedback effects can be suppressed with a very good efficiency of at least 40 dBm.

Another method, proposed in Ref. [3], is to remove the two quarter wave plates and to keep just one polarizer and a NDF in order to force the lasers to operate on only one polarization. However, retroreflection is no more controlled in this case.

IV. EXPLOITING THE SYMMETRIES

A. Symmetric and antisymmetric functions

We explore the dynamic of the system assuming the same set of parameter for both lasers, i.e., $\delta x=0$, so that $\delta F_j=0$. This restriction suggests to decompose the fields into symmetric and antisymmetric combinations,

$$S=\frac{1}{2}(E_1+E_2), \tag{16}$$

$$D=\frac{1}{2}(E_1-E_2), \tag{17}$$

to take advantage of the inherent symmetries of the problem. When Eqs. (11) and (12) are expressed in terms of S and D, they lead to a pair of coupled equations where the cross coupling appears only in the nonlinearity,

$$\dot{S}=(1+i\alpha)(p-|S|^2)S+\eta e^{-i\Omega}\overline{S} -(1+i\alpha)(2|D|^2S+D^2S^*), \tag{18}$$

$$\dot{D}=(1+i\alpha)(p-|D|^2)D-\eta e^{-i\Omega}\overline{D} -(1+i\alpha)(2|S|^2D+S^2D^*). \tag{19}$$

The system (16) and (17) exhibits the usual gauge invariance under the transformation $(S,D)\rightarrow(Se^{i\phi},De^{i\phi})$, common to optical devices without phase conjugation. Another symmetry, which is trivial here since the two subsystems are identical, is the invariance under the permutation of the fields $(S,D)\rightarrow(S,-D)$ or $(E_1,E_2)\rightarrow(E_2,E_1)$.

B. Parametric representation

To study the bifurcation diagram of Eqs. (16) and (17), a parametric representation of the fields is useful, as shown in Ref. [16]. To simplify the algebra, we concentrate on the case $p=0$. We introduce two new complex functions, X and Y, defined as

$$S(s)=X(s)e^{i\omega s},$$

$$D(s)=Y(s)e^{i\omega s},$$

where ω is a free parameter. Inserting these definitions in Eqs. (18) and (19) gives

$$\dot{X}=-(1+i\alpha)[(|X|^2+2|Y|^2)X+Y^2X^*]+\eta e^{-i(\Omega+\omega)}\overline{X} -i\omega X, \tag{20}$$

$$\dot{Y}=-(1+i\alpha)[(|Y|^2+2|X|^2)Y+X^2Y^*]-\eta e^{-i(\Omega+\omega)}\overline{Y} -i\omega Y. \tag{21}$$

This transformation allows the mapping of periodic and quasiperiodic solutions of Eqs. (18) and (19) onto steady and periodic solutions of Eqs. (20) and (21). As stressed in Ref. [16], this parametric representation is not unique. If $(X(s),Y(s),\omega)$ is a solution of Eqs. (20) and (21), the one-parameter family $(X^*(s),Y^*(s),\omega^*)$ defined by

$$X^*(s)=e^{i(\omega-\omega^*)s}X(s), \tag{22}$$

$$Y^*(s)=e^{i(\omega-\omega^*)s}Y(s), \tag{23}$$

where ω^* is an arbitrary real number, may also verify Eqs. (20) and (21). This is because all members of the family $(X^*(s),Y^*(s),\omega^*)$ correspond to the same physical solution $(E_1(s),E_2(s))$. For the steady state solutions of Eqs. (20) and (21), i.e., when $X(s)$ and $Y(s)$ are time independent, it follows from Eqs. (22) and (23) that the parametric representation is unique, i.e., $\omega=\omega^*$, while if $X(s)$ and $Y(s)$ are T_p-periodic solutions, ω and ω^* are only constrained by the relation

$$\omega^*=\omega+2k\frac{\pi}{T_p},$$

where k is an integer.

V. EXTERNAL CAVITY MODES

In this section, we analyze the plane wave solutions of Eqs. (16) and (17), which are the simplest nontrivial solutions of these equations. These periodic states are the steady states of Eqs. (20) and (21) in the parametric representation. From the structure of these equations, it follows directly that solutions with the same constant intensity for both fields must be either in phase or dephased by π. In addition, asymmetric modes exist that break the symmetry of the equations.

Strictly speaking, there are no external cavity modes because there is no external cavity and therefore no feedback at all. Still, we use this term to designate the steady state solutions of Eqs. (20) and (21) because they are algebraically very close to the external cavity modes of a semiconductor laser with external mirror. The formal analogy stems from

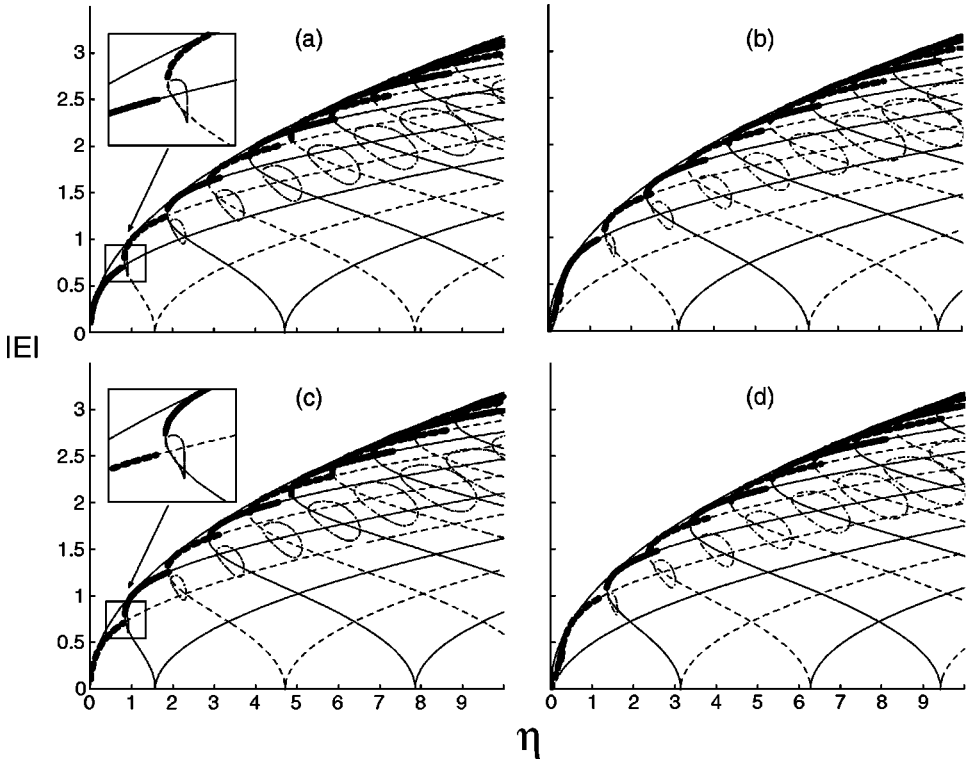

FIG. 2. Bifurcation diagram of the external cavity mode solutions. Symmetric modes are in full lines, antisymmetric modes are in dotted line, asymmetric modes are the loops in dash-dotted lines. Thick lines indicate stable solutions, thin lines indicate unstable solutions. (a) $\Omega=0$; (b) $\Omega=\pi/2$; (c) $\Omega=\pi$; (d) $\Omega=3\pi/2$. Common parameters for all figures: $\alpha=3$ and $p=0$. The insets in (a) and (c) are focused on the first asymmetric solution.

the mutual injection which leads to a generalization of the reduced Lang-Kobayashi equations [15] which are valid in the case of weak feedback, that is if there is only one reflection against the external mirror. The other justification for using this terminology is that the bifurcation diagram of these steady states has much in common with the bifurcation diagram of Eq. (15).

A. Symmetric and antisymmetric modes

The symmetric external cavity modes (S modes) are $(X(s),Y(s),\omega)=(\rho_x,0,\omega)$. Inserting this definition in Eqs. (20) and (21) leads to the relations

$$\rho_x^2=\eta\cos(\omega+\Omega), \tag{24}$$

$$\omega=-\eta[\alpha\cos(\omega+\Omega)+\sin(\omega+\Omega)]. \tag{25}$$

The antisymmetric external cavity modes (AS modes), defined by $(X(s),Y(s),\omega)=(0,\rho_y,\omega)$, lead to the steady state relations

$$\rho_y^2=-\eta\cos(\omega+\Omega), \tag{26}$$

$$\omega=\eta[\alpha\cos(\omega+\Omega)+\sin(\omega+\Omega)]. \tag{27}$$

We first consider the case $\Omega=0$. A single branch of external cavity mode emerges from a Hopf bifurcation at $\eta=0$. This solution is a S mode which is stable in the vicinity of the bifurcation point where it is supercritical. It can be approximated for $\eta\ll1$ by $(\rho_x^2,0,\omega)\simeq(\eta,0,-\alpha\eta)$. Increasing the feedback strength η, pairs of S modes emerge from Hopf bifurcations on the trivial solution $\rho=0$ located at $\eta_k=3\pi/2+2k\pi$ where k is a positive integer. In the vicinity of the bifurcation point at η_k, the first branch of the pair can be expressed as $[\rho_x^2,0,\omega]\simeq[\epsilon\eta_k/(1+\alpha\eta_k),0,\eta_k]$ provided that $\epsilon=\eta-\eta_k\ll1$ is positive. The other branch is given by $[\rho_x^2,0,\omega]\simeq[\epsilon\eta_k/(1-\alpha\eta_k),0,-\eta_k]$. It should be noticed that the first solution is always supercritical while the second branch can be either super- or subcritical, depending of the sign of $1-\alpha\eta_k$. In a similar way, pairs of AS modes emerge from the trivial solution from another set of bifurcation points $\eta_k=\pi/2+2k\pi$. The expression of ρ_y^2 for AS modes is the same as the expression of ρ_x^2 for the S modes. The properties of the bifurcations leading to the S and to the AS modes are the same. These results are summarized in Fig. 2(a). For all the figures, $\alpha=3$ and $p=0$.

For $\Omega=\pi/2$, a mixed pair of (S, AS) modes emerges at the origin $(\rho,\eta)=(0,0)$ as shown in Fig. 2(b). For $\eta\ll1$, the S mode can be approximated by $[\rho_x,0,\omega]\simeq[\eta^2(1+\alpha\eta),0,-\eta]$ and the AS mode by $[0,\rho_y,\omega]\simeq[0,\eta^2(1-\alpha\eta),\eta]$. These branches are both stable and supercritical and they merge at the origin. This is shown in Fig. 3(b). As η increases, other mixed pairs emerge from the trivial solution at the bifurcation points $\eta_k=k\pi$, k being a positive integer. For those pairs, the S mode can be expressed as $[\rho_x^2,0,\omega]\simeq\{\epsilon\eta_k/[1-\alpha\eta_k(-1)^k],0,-\eta_k(-1)^k\}$ and the AS mode by $[0,\rho_y^2,\omega]=\{0,\epsilon\eta_k/[1+\alpha\eta_k(-1)^k],\eta_k(-1)^k\}$ where $\epsilon=\eta-\eta_k\ll1$. For the parameters $\alpha=3$ and $p=0$, we have $\alpha>-1/\eta_1$. Thus, close to the bifurcation from which they emerge, the S modes are supercritical (subcritical) and the AS modes subcritical (supercritical) if k is odd (even).

Finally, it follows from the definition of the S and AS modes, Eqs. (24) and (25) and Eqs. (26) and (27), respectively, that adding π to Ω is equivalent to the mode permutation S$\rightleftarrows$AS. Thus the considerations for $\Omega=0$ and $\pi/2$

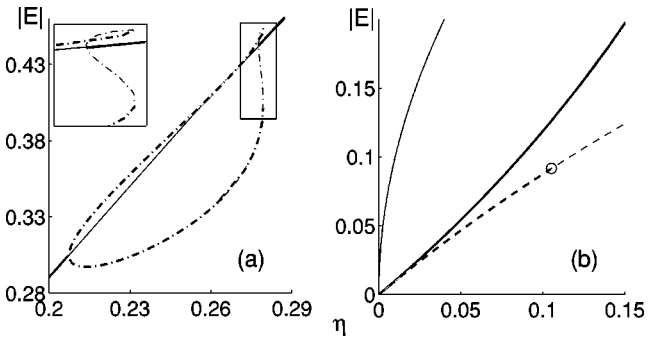

FIG. 3. Expanded view of Fig. 2(b) for $\Omega=\pi/2$ close to the origin. (a) Detail of the first loop of asymmetric modes (dashed-dotted line). The thick lines are stable states, the thin lines are unstable states. There is a small domain of bistability between the symmetric and asymmetric modes in the upper part of the loop. (b) Merging of the mixed pair of solutions at the origin. The stable S mode is the thick full line, the AS mode is the dashed line which is stable close to the origin (thick dashes) and becomes unstable via a Hopf bifurcation marked by a circle, the emerging periodic orbit is not drawn. The upper thin line is $|E|=\sqrt{\eta}$ which is the maximum that the field amplitudes can reach.

apply to $\Omega=\pi$ and $3\pi/2$, respectively, after exchanging symmetric and antisymmetric modes. In this way, Figs. 2(c) and (d) are generated from Figs. 2(a) and (b). In Fig. 2, the stability off all the steady state branches has been indicated. One more information about the stability appears in that figure. All branches which emerge subcritically from the trivial solution end at a limit point where they acquire a positive slope. Near the limit point, the new branch of solutions is always stable and loses stability at a Hopf bifurcation. The method followed to determine the stability of these solutions is given in Sec. VII.

B. Extrema

The maximum steady state intensity allowed by Eqs. (24) and (25) and (26) and (27) is either $\rho_x^2=\eta$ or $\rho_y^2=\eta$. It is reached for special values of the parameters, since η and ω must verify

$$\omega_n=-[(2n+\xi)\pi+\Omega],$$

$$\eta_n=-\omega_n/\alpha,$$

where $\xi=0$ for the S modes and $\xi=1$ for the AS modes. For these values of ω_n the phases of the S (AS) modes increase by an even (odd) number of half period during one time lag since $\omega=\omega_n$ implies $E_j(s-1)=E_j(s)$. These maxima are reached by the modes with $\omega_k<0$ if $\eta>0$ and by the modes with $\omega_k>0$ if $\eta<0$. These relations imply that the maximum intensity of the S and AS modes are interleaved periodically and separated by $\delta\eta=\pi/\alpha$. The interval $\delta\eta$ depends on α only, while Ω defines the position of the first maximum. The intensity difference between two maxima is equal to the variation of η: $\delta I=\delta\eta$. Therefore in any given interval $[0,\eta_{\max}]$ of η, there will be p modes with negative frequency, where p is the integer part of $\alpha\eta_{\max}/\pi$. The curve $\rho^2=\eta$ is drawn in Fig. 2. It is more visible in the expanded view displayed in Fig. 3(b).

C. Asymmetric modes

Solutions of a differential equation which is invariant under a symmetry group do not necessarily share that symmetry property. In this section, we analyze the existence of symmetry-breaking steady state solutions, where neither the S nor the AS components vanish:

$$X(s)=\rho_x,$$

$$Y(s)=\rho_y e^{i\phi}.$$

For this purpose we use the equivalent representation (E_1,E_2), which leads to simpler expressions. Inserting the nontrivial asymmetric solution

$$E_1(s)=\rho_1 e^{i\omega t},$$

$$E_2(s)=\rho_2 e^{i\omega t}e^{i\theta}$$

into Eqs. (11) and (12) and equating real and imaginary parts leads to

$$\rho_1^3=\eta\rho_2\cos[\theta-(\omega+\Omega)], \tag{28}$$

$$\rho_2^3=\eta\rho_1\cos[\theta+(\omega+\Omega)], \tag{29}$$

$$0=\omega\rho_1+\alpha\rho_1^3-\eta\rho_2\sin[\theta-(\omega+\Omega)], \tag{30}$$

$$0=\omega\rho_2+\alpha\rho_2^3+\eta\rho_1\sin[\theta+(\omega+\Omega)]. \tag{31}$$

Equations (28)–(31) are also verified by the S and the AS modes, for which $\rho_1=\rho_2=\rho$ and $\theta=0$ or π, respectively. The asymmetric modes are drawn in Fig. 2. For $\Omega=0$ and π, the first loop is magnified in the inset. For $\Omega=\pi/2$, a magnification of the loop formed by the asymmetric mode closest to the origin is displayed in Fig. 3(a) with an indication of its stability. This first loop is somewhat atypical and Fig. 4 shows the second loop which is the scaled model of all other asymmetrical loops. Another difference is that all the asymmetric loops, except the first one for $\Omega=\pi/2$, are entirely unstable. If $\Omega=\pi/2$, there is in the first asymmetric loop at least one stable branch. Close to the upper end of that loop, there is little domain of bistability between the asymmetric and the symmetric branches, as shown in the inset of Fig. 3(a).

Equations (28)–(31) were solved numerically. As shown in Fig. 2, the asymmetric solutions with $\theta\neq 0$ or π and $\rho_1\neq\rho_2$ always emerge from an S or an AS solution, never from the trivial solution. They also do not form isolas, i.e., branches of solutions isolated from other branches. This suggests a perturbative analysis to find the condition of emergence of asymmetric modes. Using the invariance of Eqs. (28)–(31) under the transformation $(\eta,\theta)\rightarrow(-\eta,\theta+\pi)$, we may restrict the analysis to values of θ close to zero, that is, to the asymmetric modes emerging from the symmetric external cavity modes. The solutions branching from the AS

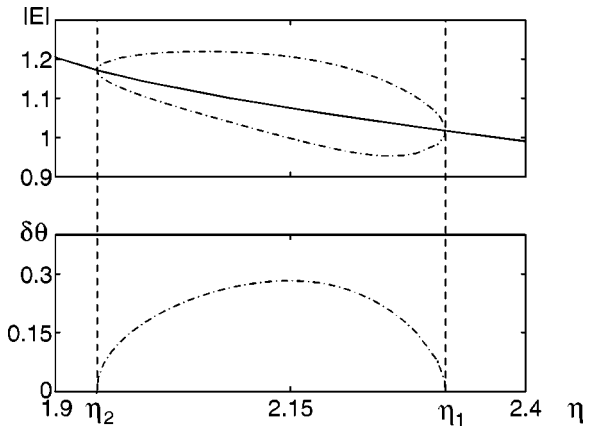

FIG. 4. Expanded view of the second loop in Fig. 2(a). There are two steady bifurcations at η_1 and η_2. The full line is the unstable steady state. For the field amplitude $|E|$, there is a degeneracy: the upper trace refers either to $E_1(\theta)$ or $E_2(-\theta)$ and the lower trace refers to either $E_2(\theta)$ or $E_1(-\theta)$, respectively.

modes are simply deduced by changing η into $-\eta$. We define a small parameter ϵ and a vicinity of the bifurcation by

$$\eta=\eta_0+\epsilon^2\delta\eta,$$

$$\theta=0+\epsilon\delta\theta+O(\epsilon^2),$$

$$\omega=\omega_0+\epsilon^2\delta\omega+O(\epsilon^3),$$

$$\rho_1=\rho_0+\epsilon\delta\rho+O(\epsilon^2),$$

$$\rho_2=\rho_0-\epsilon\delta\rho+O(\epsilon^2).$$

From Eqs. (28)–(31) we have, up to first order, the following system:

$$0=I_0+\epsilon I_1+O(\epsilon^2), \tag{32}$$

$$0=I_0-\epsilon I_1+O(\epsilon^2), \tag{33}$$

$$0=H_0+\epsilon H_1+O(\epsilon^2), \tag{34}$$

$$0=H_0-\epsilon H_1+O(\epsilon^2), \tag{35}$$

where the I_j and H_j are defined as

$$I_0=\rho_0^3-\eta_0\rho_0\cos(\omega_0+\Omega), \tag{36}$$

$$I_1=3\rho_0^2\delta\rho-\eta_0[\delta\theta\rho_0\sin(\omega_0+\Omega)-\delta\rho_0\cos(\omega_0+\Omega)], \tag{37}$$

$$H_0=\{\omega_0\rho_0+\eta_0[\alpha\cos(\omega_0+\Omega)+\sin(\omega_0+\Omega)]\rho_0\}, \tag{38}$$

$$H_1=\omega_0\delta\rho+\eta_0\{\delta\theta[\alpha\sin(\omega_0+\Omega)-\cos(\omega_0+\Omega)]\rho_0 - \delta\rho[\alpha\cos(\omega_0+\Omega)+\sin(\omega_0+\Omega)]\}. \tag{39}$$

The structure of Eqs. (32)–(35) implies that the solution is $I_j=H_j=0$. The solution $I_0=H_0=0$ is nothing else than the locus of the S mode and is verified at the bifurcation point. Since $I_1=H_1=0$ is a homogeneous system of two equations involving the two variables $\delta\theta$ and $\delta\rho$, we impose the vanishing of the determinant of this system in order to have $(\delta\theta,\delta\rho)\neq(0,0)$ at order ϵ. Using the property $I_0=H_0=0$ we find that the condition to be verified to have an asymmetric mode emerging from a S branch is

$$2\eta_0[\alpha\sin(\omega+\Omega)-\cos(\omega+\Omega)]+\omega\tan(\omega+\Omega)=0. \tag{40}$$

For the asymmetric branches emerging from the AS modes, the condition is

$$2\eta_0[\alpha\sin(\omega+\Omega)-\cos(\omega+\Omega)]-\omega\tan(\omega+\Omega)=0, \tag{41}$$

with η and ω verifying Eqs. (26) and (27).

One of these asymmetric solutions is displayed in Fig. 4 for $\Omega=0$. In the domain $\eta>\eta_1$, the solution is symmetric and the two fields have equal amplitudes. At the first bifurcation point $\eta=\eta_1$, the amplitude of one of the fields grows as the other decreases while the phase difference becomes nonzero. At the second bifurcation point, located at $\eta=\eta_2$, both moduli are again equal and the phase shift between the fields vanishes again. The system being invariant under a permutation of the two fields, there is another symmetry breaking solution obtained from the permutation $E_1\rightleftarrows E_2$. It generates the same loop for the moduli but θ should be changed into $-\theta$. All the branches displayed in Fig. 4 are unstable. This is not true for Fig. 3(a) where the bifurcation diagram is calculated for $\Omega=\pi/2$. Between the two bifurcation points ($\eta_1\leqslant\eta\leqslant\eta_2$, the S mode is unstable and the asymmetric mode is stable. Moreover, there is a small domain where both the S mode and the AS mode coexist as stable solutions.

VI. PERIODIC SOLUTIONS

A. Characteristic equation

In the previous sections, we have discussed the steady state solutions of Eqs. (20) and (21). As the feedback strength η increases, all branches eventually become unstable via a Hopf bifurcation. In this section, we focus on these bifurcation points. We seek the conditions for a periodic solution of Eqs. (20) and (21) to emerge from a steady states external cavity mode. For that purpose, we assume that the periodic solution is emerging from a S mode. The AS case is treated in exactly the same way. We perform a multiple time scale analysis in the vicinity of the Hopf bifurcation as follows. We define the small parameter $0<\epsilon\ll 1$ as the deviation from the steady state

$$\eta=\eta_0+\epsilon^2\delta\eta,$$

and the slow time scale

$$\sigma=\epsilon^2 s.$$

Treating the two times as independent, the differential operator is decomposed using the chain rule

$$\frac{d}{ds} = \partial_s + \epsilon^2 \partial_\sigma .$$

With these definitions, the X and Y components of the fields in the parametric representation, Eqs. (20) and (21), can be expanded in powers of ϵ

$$X(s,\sigma) = X_0 + \epsilon X_1(s,\sigma) + \epsilon^2 X_2(s,\sigma) + \ldots ,$$

$$Y(s,\sigma) = 0 + \epsilon Y_1(s,\sigma) + \epsilon^2 Y_2(s,\sigma) + \ldots .$$

At order zero, Eqs. (20) and (21) lead to the steady state solution (26) and (27). The first order in ϵ leads to the differential equations

$$\partial_s X_1 = -(1+i\alpha)[2|X_0|^2 X_1 + X_0^2 X_1^*] + \eta e^{-i(\Omega+\omega)}\overline{X_1} - i\omega X_1 , \tag{42}$$

$$\partial_s Y_1 = -(1+i\alpha)[2|X_0|^2 Y_1 + X_0^2 Y_1^*] - \eta e^{-i(\Omega+\omega)}\overline{Y_1} - i\omega Y_1 . \tag{43}$$

At the Hopf bifurcation, we seek solutions for $X_1(s,\sigma)$ and $Y_1(s,\sigma)$ describing undamped oscillations on the fast time scale s and amplitudes varying on the slow time scale σ:

$$X_1(s,\sigma) = \rho_x^+(\sigma) e^{i\omega_H s} + \rho_x^-(\sigma) e^{-i\omega_H s}, \tag{44}$$

$$Y_1(s,\sigma) = \rho_y^+(\sigma) e^{i\omega_H s} + \rho_y^-(\sigma) e^{-i\omega_H s}. \tag{45}$$

The compatibility condition for a nontrivial solution (44) and (45) factorizes into a product of two determinants

$$\det \mathcal{M}(\eta) \det \mathcal{M}(-\eta) = 0.$$

$\mathcal{M}(\pm\eta)$ are matrices defining the $\rho_x^\pm$ and $\rho_y^\pm$ coefficients. The factorization of the compatibility condition is obvious since Eqs. (42) and (43) are independent. This independence is a property of the field's decomposition into symmetric and antisymmetric components. The determinant of $\mathcal{M}(\eta)$ is

$$\begin{aligned}\det \mathcal{M}(\eta) = {} & [i(\omega+\omega_H) + 2(1+i\alpha)\rho_x^2 - \eta e^{-i(\Omega+\omega+\omega_H)}] \\ & \times [-i(\omega-\omega_H) + 2(1-i\alpha)\rho_x^2 - \eta e^{i(\Omega+\omega-\omega_H)}] \\ & - (1+\alpha^2)\rho_x^4 .\end{aligned}$$

Let us show that the two determinants cannot vanish simultaneously. It is easy to verify that $\det \mathcal{M}(\eta)$ and $\det \mathcal{M}(-\eta)$ are second order polynomials in η,

$$\det \mathcal{M}(\pm\eta) = A \pm B\eta + C\eta^2,$$

where A, B, and C are complex functions of $\omega, \omega_H, \alpha, \rho_x^2$, and Ω. A necessary condition to have $\det \mathcal{M}(\pm\eta) = 0$ is $B = 0$. Using the steady state relations (26) and (27), the condition $B = 0$ becomes

$$\omega_H \cos(\Omega+\omega) = 0,$$

$$\omega \sin(\Omega+\omega) + 2\eta = 0.$$

If ω_H is nonzero, it follows from Eq. (26) that $\rho_x = \eta = \omega = 0$. Thus, this necessary condition is verified only at the origin of the bifurcation diagram where it is also sufficient. Everywhere else, the vanishing of one determinant implies that the other determinant does not vanish.

B. Phase relations in the vicinity of the Hopf bifurcations

We have to distinguish two cases: either $\det M(\eta) = 0$ and $\det M(-\eta) \neq 0$ or $\det M(-\eta) = 0$ and $\det M(\eta) \neq 0$.

If $\det \mathcal{M}(\eta) = 0$, $(\rho_x^+(\sigma), \rho_x^-(\sigma))$ is an eigenvector of $\mathcal{M}(\eta)$. Since $\det \mathcal{M}(-\eta) \neq 0$, we have $(\rho_y^+(\sigma), \rho_y^-(\sigma)) = (0,0)$ and therefore $Y_1(s,\sigma) = 0$. The two fields are identical up to first order in ϵ, i.e., $E_1(s,\sigma) = E_2(s,\sigma) + O(\epsilon^2)$ with

$$\begin{aligned} E_1(s,\sigma) &= S(s,\sigma) + D(s,\sigma) + O(\epsilon^2) \\ &= \{X_0 + \epsilon X_1(s,\sigma)\} e^{i\omega s} + \{0 + \epsilon Y_1(s,\sigma)\} e^{i\omega s} + O(\epsilon^2) \\ &= \{\rho_x + \epsilon[\rho_x^+(\sigma) e^{i\omega_H s} + \rho_x^-(\sigma) e^{-i\omega_H s}]\} e^{i\omega s} + O(\epsilon^2). \end{aligned} \tag{46}$$

If $\det \mathcal{M}(-\eta) = 0$, $(\rho_y^+(\sigma), \rho_y^-(\sigma))$ is an eigenvector of $\mathcal{M}(-\eta)$ and $X_1(t,\sigma) = 0$. This implies that the two fields

$$\begin{aligned} E_1(s,\sigma) &= S(s,\sigma) + D(s,\sigma) \\ &= \{\rho_x + \epsilon[\rho_y^+(\sigma) e^{i\omega_H s} + \rho_y^-(\sigma) e^{-i\omega_H s}]\} e^{i\omega s} + O(\epsilon^2), \end{aligned} \tag{47}$$

$$\begin{aligned} E_2(s,\sigma) &= S(s,\sigma) - D(s,\sigma) \\ &= \{\rho_x - \epsilon[\rho_y^+(\sigma) e^{i\omega_H s} + \rho_y^-(\sigma) e^{-i\omega_H s}]\} e^{i\omega s} + O(\epsilon^2), \end{aligned}$$

oscillate with a phase mismatch

$$E_2(s,\sigma) e^{i\phi} = E_1\left(s + \frac{T_H}{2}, \sigma\right) + O(\epsilon^2)$$

with $\phi = \pi\omega/\omega_H$.

Therefore Hopf bifurcations can occur on symmetric modes to give symmetric periodic solutions (46) as in Ref. [15]. However, symmetry breaking bridges of periodic solutions (47) can also emerge from perfectly synchronized states. This requires that the two lasers start to describe the same periodic trajectory in the phase space but with a phase mismatch. As there are only two eigenvalues which cross the imaginary axis, the only way for the system to break the symmetry is via such a phase mismatch. Straightforward calculations show that the above results still hold at the second order in ϵ.

C. Two modes approximation and the bridges formation mechanism

Bridges connecting steady solutions with the same symmetry have been analyzed in Ref. [17] and this analysis is applicable here without significant modifications. We extend this analysis to study bridges that connect symmetric and antisymmetric solutions. Let $E_1(s)$ and $E_2(s)$ be written as

$$E_1(s)=S(s)+D(s),$$

$$E_2(s)=S(s)-D(s),$$

with

$$S(s)=\rho_s e^{i\omega_s s},$$

$$D(s)=\rho_d e^{i\omega_d s}.$$

The nonlinear term in Eqs. (11) and (12) are

$$|E_1|^2E_1=\rho_s e^{i\omega_s s}[|\rho_s|^2+2|\rho_d|^2]+\rho_d e^{i\omega_d s}[|\rho_d|^2+2|\rho_s|^2]+\text{h.h.},$$

$$|E_2|^2E_2=\rho_s e^{i\omega_s s}[|\rho_s|^2+2|\rho_d|^2]-\rho_d e^{is\omega_d s}[|\rho_d|^2+2|\rho_s|^2]+\text{h.h.},$$

where h.h. stands for higher order harmonics. Equating the term in $e^{i\omega_s s}$ and $e^{i\omega_d s}$ in Eqs. (11) and (12) separately gives the two complex equations

$$i\omega_s\rho_s=-(1+i\alpha)[|\rho_s|^2+2|\rho_d|^2]\rho_s+\eta e^{-i(\Omega+\omega_s)}\rho_s,$$

$$i\omega_d\rho_d=-(1+i\alpha)[|\rho_d|^2+2|\rho_s|^2]\rho_d-\eta e^{-i(\Omega+\omega_d)}\rho_d.$$

Assuming $\rho_s\rho_d\neq 0$, a further simplification is

$$|\rho_s|^2=\eta[2\ \cos(\Omega+\omega_d)+\cos(\Omega+\omega_s)]/3, \quad (48)$$

$$|\rho_d|^2=\eta[2\ \cos(\Omega+\omega_s)+\cos(\Omega+\omega_d)]/3, \quad (49)$$

$$0=\omega_s+\eta[\alpha\ \cos(\Omega+\omega_s)+\sin(\Omega+\omega_s)], \quad (50)$$

$$0=\omega_d-\eta[\alpha\ \cos(\Omega+\omega_d)+\sin(\Omega+\omega_d]. \quad (51)$$

Figure 5 shows that the agreement between the analytical result (48)–(51) and a numerical simulation is very good. Note that this approximation breaks down if the two frequencies ω_s and ω_d are too close of each other, i.e., if combination tones can interfere with either ω_s or ω_d.

VII. NUMERICAL RESULTS

We have analyzed numerically the reference model using a continuation algorithm adapted to delayed differential equations [18]. This leads to a bifurcation diagram of all steady and periodic solutions of Eqs. (20) and (21). Figure 6 shows the bifurcation diagram including all steady and periodic solutions, with an indication of their stability (thick lines). More complex solutions such as quasiperiodic or chaotic solutions are not drawn on this diagram. They cannot be obtained from this algorithm.

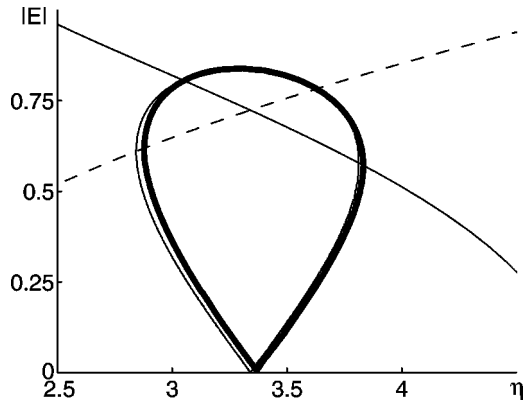

FIG. 5. Comparison between the analytical approximation (thin line) and the numerical result (thick line) for the bridge connecting a symmetric and an antisymmetric steady state. The upper (lower) part of the bridge emerging from the steady states is the maximum (minimum) amplitude of the periodic solution. Full line: symmetric steady state. Dashed line: antisymmetric steady state.

From the origin $\rho=\eta=0$, a stable steady state emerges. If $\Omega=0$ or π, that steady state is unique. It is symmetric for $\Omega=0$ and antisymmetric for $\Omega=\pi$. If $\Omega=\pi/2$ or $3\pi/2$, a pair of symmetric and antisymmetric solutions emerge. They are both stable very close to the origin [Fig. 3(b)]. For $\Omega=\pi/2$ (respectively $3\pi/2$), it is the AS (respectively S) mode that becomes unstable first via a Hopf bifurcation. The coexistence of stable solutions emerging from the same bifurcation point results from the degeneracy of all the bifurcations of the trivial solution, as analyzed in Ref. [15].

Branches of periodic solutions usually form bridges, as shown in Refs. [17,19]. These bridges can connect either branches of the same symmetry (S to S and AS to AS), or branches of different symmetries (S to AS). In Fig. 6, the bridges of periodic solutions should not be confused with the loops of asymmetric steady state solutions which already appear in Fig. 2. The mechanism which generates these bridges of periodic solutions has been described in Refs. [17,19]. In

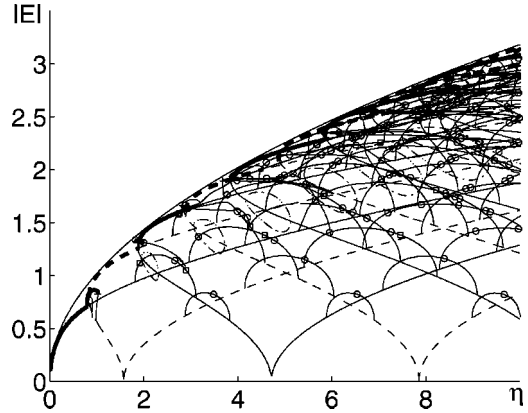

FIG. 6. The complete bifurcation diagram for the steady and the periodic external cavity mode solutions with $\Omega=0$. Same graphical convention as in Fig. 2.

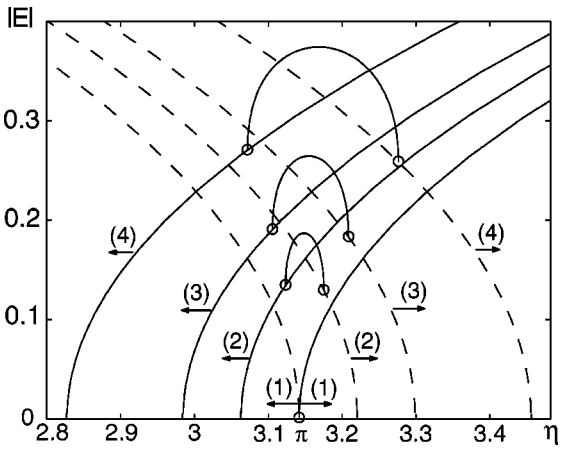

FIG. 7. Birth of a bridge of periodic solutions connecting a symmetric and an antisymmetric bridge. (1)$\Omega=10\pi/20$; (2)$\Omega=11\pi/20$; (3)$\Omega=12\pi/20$; (4)$\Omega=14\pi/20$. Steady and periodic solutions are all unstables in this figure.

Ref. [15], a mechanism of bridge destruction has been found, that leads from bridges of periodic solutions to open branches of periodic solutions. All these results apply to this problem, without any change, to bridges connecting solutions of the same symmetry. We show in Fig. 7 that the mechanism of bridges formation can be extended to the mixed periodic solutions connecting an S and an AS mode. This bridge can emerge only at a point where the S and AS modes coincide. This is the case for $E_1(s)=E_2(s)=0$ only. As $\Omega=\varepsilon+\pi/2$ and $\varepsilon\to 0^+$, the two Hopf bifurcations limiting the bridge of periodic solutions on the S and AS branches approach the axis $|E|=0$ and at $\varepsilon=0$ they merge with the Hopf bifurcations from which the S and the AS branches emerge. Thus for $\varepsilon\to 0^+$ four Hopf bifurcations coincide, while for $\varepsilon\to 0^-$ there are only two Hopf bifurcations. This indicates the complexity of the bifurcation point at $\Omega=\pi/2$.

Another feature of the periodic solutions found in the reference problem (20) and (21) is the occurrence of a homoclinic solution. Figure 8 shows the vicinity of a homoclinic point for $\Omega=0$. From the second loop of

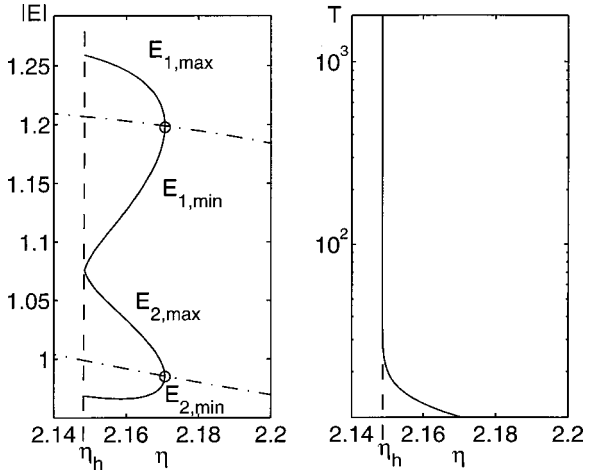

FIG. 8. Vicinity of the homoclinic solution at η_h for $\Omega=\pi$.

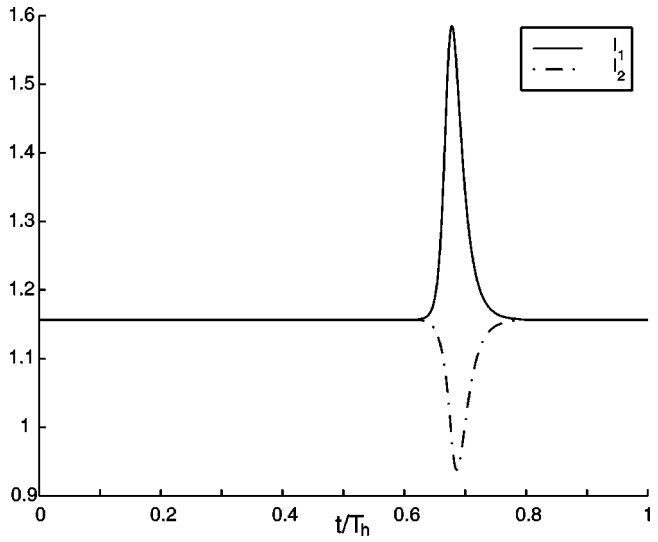

FIG. 9. Profile of the homoclinic connection in terms of the intensity of the two fields. The period of the solution is $T_h \simeq 2000$.

asymmetric solutions (counting from the origin) a Hopf bifurcation, indicated by a little circle in the figure, produces a branch of periodic solutions with $E_1\neq E_2\neq 0$. The amplitude of the oscillations grows from zero at the bifurcation until the homoclinic point where $E_{1,\max}=E_{2,\min}$ and where the period diverges.

Although there is no obvious fit of the numerical solutions displayed in Fig. 9, the decomposition of the solutions in terms of the $|S|$ and Φ_s functions displayed in Fig. 10 is very well approximated by classical soliton profiles

$$|S|=A_0+A_1\left[1-\tanh^2\left(\frac{t-t_0}{T_h}\right)\right],$$

$$\Phi_S=A_2\frac{t}{T}+A_3\tanh\left(\frac{t-t_1}{T_h}\right).$$

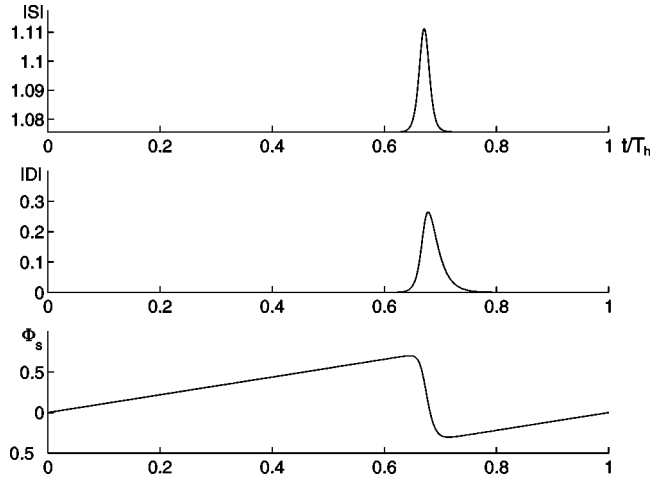

FIG. 10. Same as in Fig. 9 but in terms of the S and AS components of the fields.

However, there is no simple approximation for $|D|$ because its profile is too asymmetric. We did not pursue the search of a good fit further since the branch of periodic solutions and its homoclinic limiting point are anyway unstable.

VIII. CONCLUSION

In this paper, we have studied a model for single mode lasers coupled in a F2F configuration. The model can be derived from the Maxwell-Bloch equations, assuming that the material polarization can be adiabatically eliminated and that the two lasers are far away from each other. In addition, each laser is assumed to be pumped close to the lasing threshold of the isolated laser. The resulting equations are Eqs. (11) and (12). The same equations are obtained in the same large delay limit for semiconductor lasers coupled F2F. There is also the implicit assumption that any refection of a beam from the incoupling mirror of the other laser is either negligible or canceled by a dedicated setup. This can be achieved, for instance, with polarized light.

This paper focuses on the properties of the periodic and quasiperiodic solutions of Eqs. (11) and (12). The analysis is made possible because these solutions correspond to the steady and periodic solutions of a set of equations obtained from Eqs. (11) and (12) by a unitary transformation. In addition, we have found a homoclinic point and solutions in its vicinity are also described. Much of the analysis is numerical, though analytic results are presented whenever possible and new. The solutions for identical lasers coupled F2F can be classified according to their symmetry properties under a permutation $E_1 \rightleftarrows E_2$. There are symmetric, antisymmetric, and asymmetric solutions. The properties of the symmetric solutions are similar to those of the Lang-Kobayashi equations in the long delay time limit and have already been studied in Ref. [15]. They are not repeated here. With minor changes, the same analyses apply also to the antisymmetric solutions and therefore they are also not presented here. The new feature of the coupled Eqs. (11) and (12), compared to the single delay differential equation studied in Ref. [15], is therefore the asymmetric solutions which can be of two different kinds, either steady state loops or periodic bridges.

It is seen in Fig. 6 that even if the bifurcation diagram is restricted to steady and periodic solutions, it is extremely complex. Although most of the solutions are unstable, it is necessary to draw them to understand the origin of the stable branches. This is especially clear with the branches of steady state emerging subcritically from the trivial solutions as unstable solutions. All these branches become stable over a finite interval of the scaled feedback parameter η above the limit point. The other reason to display that bifurcation diagram is more pedagogical: it is to show how the addition of even a small linear but delayed term in an ordinary differential equation can deeply change its properties.

ACKNOWLEDGMENTS

We wish to acknowledge useful discussions with Koen Engelborghs. This research has been supported by the Fonds National de la Recherche Scientifique, the Interuniversity Attraction Pole Program of the Belgian government and a Marie Curie grant of the European Union.

[1] G. D. VanWiggeren and R. Roy, Int. J. Bifurcation Chaos Appl. Sci. Eng. **9**, 2129 (1999).
[2] A. Hohl, A. Gavrielides, T. Erneux, and V. Kovanis, Phys. Rev. Lett. **78**, 4745 (1997).
[3] T. Heil *et al.*, Phys. Rev. Lett. **86**, 795 (2001).
[4] J. K. White, M. Matus, and J. V. Moloney, Phys. Rev. E **65**, 036229 (2002).
[5] Y. Kuramoto, *Chemical Oscillations, Waves and Turbuence* (Springer, Berlin, 1984).
[6] S. H. Strogatz, Physica D **143**, 1 (2000).
[7] S. Kim, S. H. Park, and C. S. Ryu, Phys. Rev. Lett. **79**, 2911 (1997).
[8] D. V. R. Reddy, A. Sen, and G. L. Johnston, Phys. Rev. Lett. **80**, 5109 (1998).
[9] S. Kim, S. H. Park, and H.-B. Pyo, Phys. Rev. Lett. **82**, 1620 (1999).
[10] M. K. Yeung and S. H. Strogatz, Phys. Rev. Lett. **82**, 648 (1999).
[11] R. Lang and K. Kobayashi, IEEE J. Quantum Electron. **QE-16**, 347 (1980).
[12] P. M. Alsing, V. Kovanis, A. Gavrielides, and T. Erneux, Phys. Rev. A **53**, 4429 (1996).
[13] G. Kozyreff, A. G. Vladimirov, and P. Mandel, Phys. Rev. Lett. **85**, 3809 (2000).
[14] G. Kozyreff, A. G. Vladimirov, and P. Mandel, Phys. Rev. E **64**, 016613 (2001).
[15] D. Pieroux and P. Mandel (unpublished).
[16] B. Haegeman *et al.*, Phys. Rev. E **66**, 046216 (2002).
[17] D. Pieroux, T. Erneux, T. Luzyanina, and K. Engelborghs, Phys. Rev. E **63**, 036211 (2001).
[18] K. Engelborghs, Technical Report No. TW-305, K.U. Leuven, Leuven, Belgium (unpublished).
[19] D. Pieroux *et al.*, Phys. Rev. Lett. **87**, 193901 (2001).